Modelling of battery thermal management: A new concept of cooling using fuel

Al Qubeissi, M., Almshahy, A., Mahmoud, A., T.K. Al-Asadi, M. & Raja Ahsan Shah, R. M.

Original citation & hyperlink:
Al Qubeissi, M, Almshahy, A, Mahmoud, A, T.K. Al-Asadi, M & Raja Ahsan Shah, RM 2022, 'Modelling of battery thermal management: A new concept of cooling using fuel', *Fuel*, vol. 310, no. B, 122403.
https://dx.doi.org/10.1016/j.fuel.2021.122403

DOI 10.1016/j.fuel.2021.122403
ISSN 0016-2361

Publisher: Elsevier

Modelling of battery thermal management: A new concept of cooling using fuel

Mansour Al Qubeissi[1,2*], Ali Almshahy[1,3†], Ayob Mahmoud[1], Mushtaq T.K. Al-Asadi[3], Raja Mazuir Raja Ahsan Shah[2]

[1] *Faculty of Engineering, Environment and Computing, Coventry University, Coventry CV1 2JH, United Kingdom*

[2] Research Institute for Clean Growth and Future Mobility, *Coventry University, Coventry CV1 5FB, United Kingdom*

[3] *Basra Oil Company (BOC), Ministry of Oil, Basra, Iraq*

Abstract

Battery thermal management system (BTMS) design is crucial for its performance, which can be associated with extra costs and system complexity. Most of the current studies are focused on the BTMS design but with a little focus on the improvement of coolants. In this work, the feasibility of using combustion engine fuel for the LIB thermal management of hybrid electric vehicles is investigated. N-heptane is used as a dielectric hydrocarbon coolant in the introduced system. The thermal performance of the proposed system is investigated numerically using the CFD software ANSYS-Fluent. To benchmark and validate the system performance, a comparative study is made among other common approaches, including the use of air and 3M-Novec 7200. A variety of input parameters are accounted for, including inlet velocities and discharge rates. The results show that air cooling is the least effective method to control the battery module temperature uniformity and the Li-ion battery safety limit. At the same time, n-heptane and 3M-Novec 7200 have shown good control of the module temperature range (20 °C–40 °C) at various discharge rates and different inlet velocities. However, using n-heptane is a considerable improvement to the cost of the system and reduction in its weight and maximum temperature, compared to that using 3M-Novec 7200 coolant. For instance, at 0.1 $m \cdot s^{-1}$, n-heptane has reduced the Li-ion battery maximum temperature at 1C and 2C discharge rates by more than 7.9 °C (2.6%) and 17.9 °C (5.65%), respectively, compared to those predicted using the same battery module without cooling.

[*] 1st Corresponding author: M. Al Qubeissi, Email address: ac1028@coventry.ac.uk.
[†] 2nd Corresponding author: A. Almshahy, Email address: almshaha@coventry.ac.uk

Keywords: Battery thermal management; Electric vehicles; Fuel coolant; N-heptane; Heat transfer, Numerical analysis

Nomenclature

Abbreviation

BEV	Battery electric vehicle(s)
BTMS	Battery thermal management system(s)
CFD	Computational fluid dynamics
EV	Electric vehicle(s)
HEV	Hybrid electric vehicle(s)
ICE	Internal combustion engine(s)
LIB	Lithium-ion battery
MSMD	Multi-scale multi-domain
OCV	Open circuit voltage
SOC	Stage of charge
UDF	User defined function

Mathematical scripts

Symbol	Definition	Unit
C_p	Specific heat	$J \cdot kg^{-1} K^{-1}$
D_H	Hydraulic diameter	m
G_b	Rate of generated kinetic energy by buoyancy	W
G_K	Rate of generated kinetic energy	W
I	Discharge current	A
I_t	Turbulence intensity %	-
k	Thermal conductivity	$W \cdot m^{-1} K^{-1}$
$\dot{Q}$	Heat generation rate	W
Q_J	Joule heat	W

Q_{gen}	Heat generation	W
Q_r	Electrochemical reaction heat	W
Re	Reynolds number	-
S	Entropy	J·kg^{-1}
T	Temperature	K (or °C, as indicated)
U_{in}	Inlet velocity	m·s^{-1}
V	Cell voltage	V

Greek Symbols

μ	Dynamic viscosity	kg·m^{-1}s^{-1}
σ_k	Turbulent Prandtl number for k	-
ε_k	Turbulent Prandtl number for e	-
S_k	User defined source	-
S_k	User defined source	-
ρ	Density	kg·m^{-3}

1. Introduction

It has been believed that electric vehicles (EV) produce zero pollution and high energy utilization [1]. Recently, EV and hybrid electric vehicles (HEV) have been increasingly relied upon in the automotive industry to minimise greenhouse gas emissions and running costs [2]. For instance, 315000 BEV were sold in 2014, increased around 50% from 2013 [3]. This number reached 774,000 in 2016 with a 40% growth rate, compared to 2015, and from 754,000 in 2017 to over 1.5 million in 2019, according to ACEA [4]. Also, 12.3m BEV were produced in 2020 worldwide, where HEV alone were 15.1% of newly manufactured vehicles across the EU [4]. Therefore, BEV have undoubtedly become an important domain in the automotive industry associated with the growth rate in recent years. Therefore, lithium-ion battery (LIB) is becoming an important source of power for on-road vehicles [5,6].

Alipour et al. [7] studied the thermal and electrochemical performance of 20 Ah LiFePO4 prismatic cells at discharge rates: 0.2C−5C, in the range of operating temperatures: -20 °C −50 °C. The general trend of results in [7] shows the importance of BTMS for the high-capacity cells at higher temperatures and C-rates. That was attributed to the finding that high LIB temperature differences can lead to nonuniform material utilization, which results in cell failures. Therefore, the lifecycle of 20 Ah LIB was significantly decreased when the discharge C-rates increased.

Spitthoff et al. [8] have given a detailed overview of experimental studies on the influence of LIB operating conditions involving variety of chemical features, sizes, state of charge (SOC) and C-rates. It has been concluded that the LIB lifespan can be dependent on the reduced C-rates (i.e., at lower operation temperatures).

Liang et al. [9], investigated the selection of optimum cooling surface for prismatic LIB based on system dimensions, thermal conductivity, and metal shell. For instance, the study determined the importance of the heat transfer enhancement using aluminium shell. Also, it was shown that a double surfaced cooling system can mimic the temperature gain by up to 24.1%, compared with that using the single surfaced cooling system.

Although previous studies highlighted the importance of BTMS with varies applications and conditions, there were very limited studies on the use of novel coolants for the conventional BTMS, to the authors' knowledge. The reliance on fossil fuels can be vanishing in the coming era, due to their depletion and high pollution [2,10]. However, energy is not limited to these types of fuels only. Alternatives fuels are visioned as a bridge to the future resources of energy [11]. For instance, LIB recycle can be a major environmental challenge associated with its toxic electrolyte [12]. Hence, the rushed perceptions about BEV as the only alternative solution can be misleading [10]. Generally, EV are less powerful than vehicles powered by internal combustion engines (ICE) and can still contribute to pollutions [13]. Meanwhile, HEV is a successful response to the market yet [2,12], which can bridge the temporary gap between the ICE vehicles and EV. HEV are potentially cost-effective and beneficial in reducing emissions on the roads, compared to the pure ICE [14].

LIB heat up during their charge and discharge states. In order to preserve the safety, effectiveness, and longevity of the LIB, they need to be cooled effectively [1,15]. 3M Noves 7200 is used as a conventional dielectric coolant in these LIB thermal management system, which is, however, relatively heavy (specific density= 1.4) [16], more expensive [3], and of lower thermal conductivity [17], compared to the proposed dielectric fuel in this work. We will numerically investigate the battery thermal management systems (BTMS), using a variety of cooling techniques for temperature management. ANSYS-Fluent computational fluid dynamics (CFD) software, with a user-defined function (UDF) (see an example of the ANSYS-Fluent UDF in [18]) of the temperature dependent properties, is used in this analysis. More importantly, a dielectric fuel (used in ICE) is used as a coolant in an HEV. Such an approach can contribute to the light-weighting of HEV, in replacement to the conventional liquid coolant. This new concept of using a dielectric fuel cooling has not been presented in the literature, to the best of our knowledge. It is expected that the findings of this study can contribute to improving the thermal management efficiency and reducing the cost and weight of HEV in total. The selected fuel components are made in the LIB optimal temperature range, which is beyond these fuel flashpoints to avoid the risk of fire.

There are different length scales and different physics associated with each LIB component, which complicates the problem [19]. Due to the multi-domain and multi-physics nature of LIB, it is a challenge to provide an accurate thermal management model. When performing a thermal analysis, the goal is to determine the temperature distribution at the battery length scale. Despite having efficiencies higher than ICE, heat rejection from EV battery cells remains a challenge due to lower operating temperatures. When combining ICE and EV systems in hybrid vehicles, there is a potential of using the operating fuel as a coolant. Air-cooled BTMS is widely applied to several EV due to its simplicity and cost effectiveness [20,21]. However, air cooling in such systems may not meet the cooling requirements under high power and stressful conditions (e.g. fast discharge or charge rates) [22]. 3M-Novec 7200 is dielectric liquid, which has been widely engineered as an immersion-coolant of LIB in the EV industry. This coolant has proven its good efficiency in maintaining the system temperature in the needed range under practical operating conditions [23]. It has relatively low viscosity, non-flammability feature and high thermally conductivity [23]. N-heptane is a dielectric hydrocarbon and a dominant component of petrol (gasoline) fuel composition [24,25]. The concept of using n-heptane as an alternative to standard BTMS coolants is the first of its kind, which can improve the system efficiency, reduce its cost, and contribute to the HEV light-weighting. It can also achieve a good temperature uniformity among cells and reduce the variation in temperature across the LIB module, with less than 1°C (in this study).

This work entails a full thermal simulation to compare a highly performing widely used dielectric liquid coolant (3M novel 7200) with dielectric hydrocarbon fuel, represented by heptane, as an alternative cooling liquid. The physics governing the LIB transport in the anode-separator-cathode sandwich layers (the electrode pair length scale) are accounted for. LIB transport in an active material occurs at the atomic length scale. The Multi-Scale Multi-Domain (MSMD) approach, which is made for several physics in different solution domains, is used in this analysis. The simple semi-empirical electrochemical sub-model of Newman, Tiedemann, Gu, and Kim (NTGK) (see [26] for details about this model) is used to simulate the electro-chemistry and discharging process. The discharging process of the battery pack is occurring under both constant C-rate and transient C-rate and at a low state of charge, with a nominal cell capacity of 10 Ah. In what follows, the model and parametric set-ups are described in Section 2, the results of the studied cases and comparative analysis are presented in Section 3, and the main findings are summarised in Section 4. Relevant illustrative figures and findings are provided in Appendices A and B.

2. The model

In this work, a three-dimensional computational fluid dynamic (CFD) model has been developed using ANSYS-Fluent software (see Figures 1 and 2 for illustration). The lifespan, performance and safety of LIB are primary concerns for the industry, which are influenced by their thermal management. In our ANSYS-Fluent model, the battery module is simulated to account for the thermal and electrochemical behaviours. In a hybrid (engine and battery) power system of EV, fuel is still needed to feed the ICE. Therefore, to improve the system effectiveness, dielectric fuels can be used for cooling and feeding the ICE. In this study, three types of coolants are analysed: air, 3M-Novec 7200 [16] and n-heptane (inferred from [24,25]).

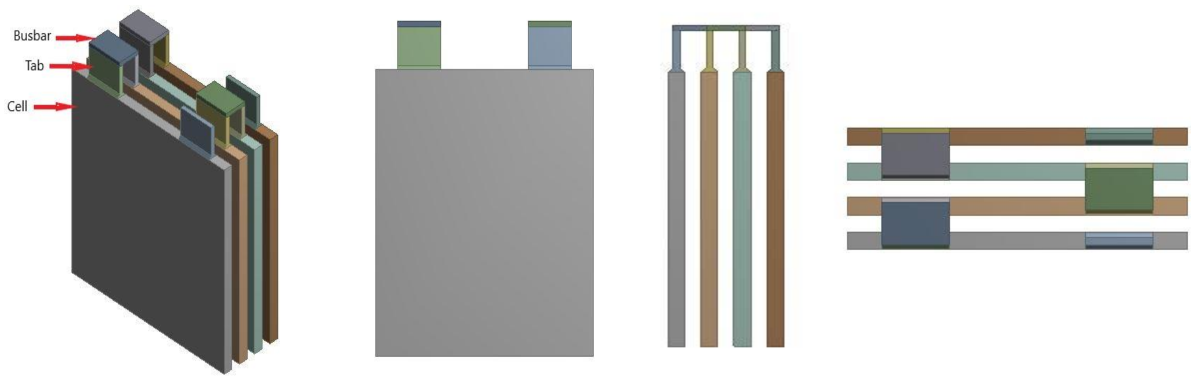

Figure 1. Schematic of the battery module, showing the isometric-view and three main side-views.

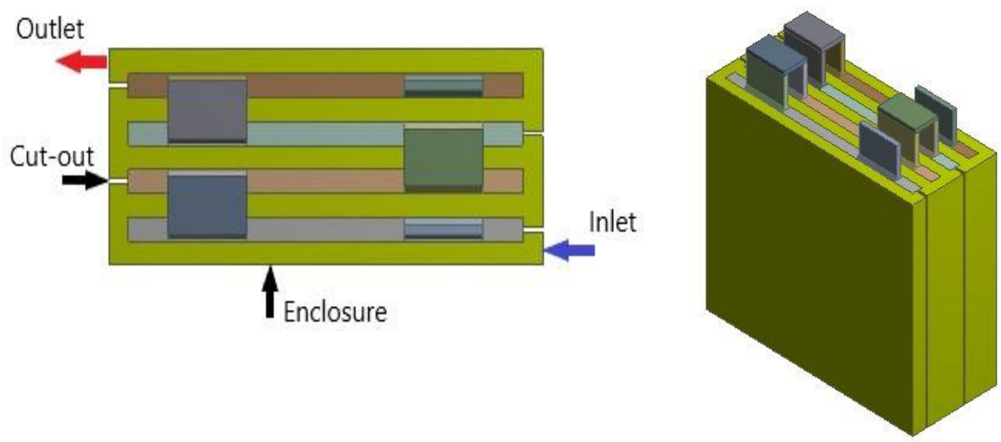

Figure 2. Top and isometric views of the battery module and enclosure.

The ANSYS-Fluent CFD tool is utilized to evaluate the power and thermal management of the LIB module under stretched ambient conditions. The LIB module and BTMS are investigated for a fluid enclosure, LIB cells, and cooling channels. The performance of BTMS is investigated in a comparative analysis, using air, 3M-Novec 7200 and n-heptane, as coolants in a direct contact flow. The system performance for each case is assessed based on the temperature distribution and values, compared to the benchmark result using the LIB module without a cooling medium. In what follows the main settings considered in the CFD model are presented.

2.1 Basic equations

The LIB is evaluated using MSMD approach with NTGL sub-model to simulate the electrochemical behaviour and power source [27]. The battery cell temperature distribution is calculated based on the energy conservation equation [28,29]:

$$\frac{\partial}{\partial t}(\rho_b C_{pb} T) = \nabla \cdot (k_b \nabla T) + Q_{\text{gen}}, \tag{1}$$

where C_{pb} is the specific heat capacity, ρ_b is the density of battery material, Q_{gen} is the battery heat generation, T is the temperature, and k_b is the thermal conductivity. The LIB cell temperature is subject to the amount of heat generation (Q_{gen}) in (1), which consists of two main sources, electrochemical reaction heat Q_r and joule heat Q_J [30]. Reaction heat can be calculated as [1]:

$$Q_r = -T\Delta S \frac{I}{nF}, \tag{2}$$

where ΔS is the change in entropy, I is the current of electric discharge, F is faraday constant (assumed in this study as 96485.0 $C \cdot \text{mol}^{-1}$), and n is the number of electrons. The dissipated Joule heat is determined as [31]:

$$Q_J = I(E - V), \tag{3}$$

where E is the open circuit voltage and V is the operating voltage. Both E and V are dependent on the battery temperature and state of charge (SOC). Thus, Q_{gen} is determined as:

$$Q_{\text{gen}} = Q_r + Q_J \equiv I(E - V) - T\Delta S \frac{I}{nF}. \tag{4}$$

The conservation of momentum for the coolant flow is calculated as:

$$\frac{\partial}{\partial t}(\rho \vec{v}) + \nabla \cdot (\rho \vec{v}\vec{v}) = -\nabla P. \tag{5}$$

The conservation of mass (continuity equation) is calculated as:

$$\frac{\partial \rho}{\partial t} + \nabla \cdot (\rho \vec{v}) = 0. \tag{6}$$

The energy equation of the coolant is expressed as [31]:

$$\frac{\partial}{\partial t}(\rho_c c_{pc} T_c) + \nabla \cdot (\rho_c c_{pc} \vec{v} T_c) = \nabla \cdot (k_c \nabla T_c), \tag{7}$$

c_{pc} is the specific heat capacity of coolant, ρ_c is the density of coolant, and $\vec{v}$ is the velocity of coolant.

The flow turbulence effects are accounted for using the kinetic energy and dissipation $(\kappa - \varepsilon)$ turbulence model, due to its simplicity and robustness for this application [32]. Using ANSYS-Fluent CFD software, the transport equation for standard turbulent kinetic energy (κ) and eddy viscosity (ε) are determined as [32]:

$$\frac{\partial \rho \kappa}{\partial t} + \nabla\left[\rho \vec{V} \kappa\right] = \nabla\left[\left(\mu + \frac{\mu_t}{\sigma_\kappa}\right)\nabla \kappa\right] + G_\kappa + G_b - \rho\varepsilon - Y_M + S_\kappa, \tag{8}$$

$$\frac{\partial \rho \varepsilon}{\partial t} + \nabla\left[\rho \vec{V} \varepsilon\right] = \nabla\left[\left(\mu + \frac{\mu_t}{\sigma_\varepsilon}\right)\nabla \varepsilon\right] + C_1 \frac{\varepsilon}{\kappa}(G_\kappa + C_3 G_b) - C_2 \rho \frac{\varepsilon^2}{\kappa} + S_\varepsilon, \tag{9}$$

where σ_ε is the eddy viscosity using the turbulent kinetic energy, σ_k is the turbulent Prandtl number, G_κ is the rate of deformation due to κ, Y_M is the turbulence kinetic energy due to the fluctuating dilatation, G_b is the turbulence kinetic energy due to buoyancy effects, respectively, the constants are assumed as $C_1 = 1.44$, $C_2 = 1.92$ and $C_3 = 0.09$, and S_κ and S_ε coefficients are user-defined sources. In this study, it turned out that the inlet turbulence of fluid has a significant impact on the prediction of downstream flow. Our analysis is based on the assumption that the coolant is fully turbulent, with a flow direction normal to the inlet surface. The level of inlet turbulence is defined by the turbulence intensity, which is dependent on the hydraulic diameter and velocity. The turbulence intensity (I_t) is calculated for each case as [33]:

$$I_t = 0.16\ \mathrm{Re}_{D_H}^{-0.125}, \tag{10}$$

where Re_{D_H} is the Reynolds number calculated for the hydraulic diameter $D_H = 0.013$ m.

2.2 System parameters and specifications

The velocity-inlet is the main defined boundary condition of the system flow field. To investigate the impact of fluid motion on the LIB thermal performance, three different inlet velocities are considered: 0.1 m·s^{-1}, 0.5 m·s^{-1} and 1 m·s^{-1}. Also, three different discharge C-rates (1C, 1.5C and 2C) are accounted for at each inlet velocity in a transient simulation, within each time-step (1s), until the battery full discharge state is reached. The inlet temperature and outlet pressure of the three coolants are assumed as 298 K ambient temperature and 1 atm ambient pressure, respectively. The heat transfer coefficient for the module is assumed equal to 5 W·m^{-2}K^{-1}. The boundary conditions for the three coolants, air, 3M-Novec 7200 and n-heptane, are shown in Table 1. The main physical properties of the three coolants at room temperature are shown in Table 2. The LIB system without cooling is considered as the benchmark case.

Table 1. Boundary conditions used in the BTMS analysis for the three cooling mediums.

Coolants	Case	Parameters			
		T_{in} (K)	u_{in} (m·s^{-1})	Re	I_t (%)
air	1	298	0.1	83.2	9.206
	2	298	0.5	416	7.529
	3	298	1	832	6.904
3M Novec	1	298	0.1	3182.75	5.838
	2	298	0.5	15913.8	4.774
	3	298	1	31827.6	4.378
n-heptane	1	298	0.1	2285.9	6.084
	2	298	0.5	11362.5	4.979
	3	298	1	22724.9	4.566

Note: I_t is calculated by using Eq. (10).

Table 2. Main thermodynamic properties of the three cooling mediums.

Properties	air	3M-Novec 7200	n-heptane
Density (kg·m^{-3})	1.184	1420	684
Specific heat ($\text{J} \cdot \text{kg}^{-1} \cdot \text{K}^{-1}$)	1007	1220	2219
Thermal conductivity (W·m^{-1}·K^{-1})	0.00255	0.068	0.14
Dynamic viscosity (kg·m^{-1}·s^{-1})	0.0000185	0.00058	0.000409

The EV LIB module used in this analysis is composed of four commercial 10 Ah prismatic LIB cells. However, the number of cells within an LIB module, and the modules within an LIB pack, can differ upon the manufacturer's preference, in response to certain design parameters. The 4-cell string module of LIB is connected in series and the total string is connected in parallel (4S1P) with aluminium tabs and copper busbars. The prismatic cells are spaced with 5 mm channels of cooling fluid to sustain a good temperature uniformity of the cells. A schematic of the LIB module was illustrated in Figure 1. The main material properties and specifications of the module are presented in Table 3.

Table 3. Specifications and material properties of the LIB module.

LIB cell specification		Busbar (Copper)	
Nominal capacity (Ah)	10		
Max voltage (V)	4.2	Density ($kg \cdot m^{-3}$)	8978
Min voltage (V)	3	Specific Heat ($J \cdot kg^{-1}K^{-1}$)	381
Max discharge rate	2C-rate (20 A)	Thermal conductivity ($W \cdot m^{-1}K^{-1}$)	387.6
Min discharge rate	1C-rate (10 A)	Electrical conductivity ($S \cdot m^{-1}$)	5.8×10^7
Height (mm)	100		
Width (mm)	100	Tab (Aluminium)	
Thickness (mm)	5	Density ($kg \cdot m^{-3}$)	2719
Gap between cells (mm)	5	Specific Heat ($J \cdot kg^{-1}K^{-1}$)	871
Density ($kg \cdot m^{-3}$)	2092	Thermal conductivity ($W \cdot m^{-1}K^{-1}$)	202.4
Specific Heat ($J \cdot kg^{-1}K^{-1}$)	678	Electrical conductivity ($S \cdot m^{-1}$)	3.541×10^7
Thermal conductivity ($W \cdot m^{-1}K^{-1}$)	18.2		

2.3 Fluid domain and meshing

The LIB module is wrapped up with the fluid enclosure for effective thermal management. In contrast to previous studies (e.g., [3,19,23,29]), where the LIB module is immersed inside a box-like enclosure or plated with indirect cooling, we have created cut-outs around the LIB cells for guided flows in this analysis. This was so much similar to the approach introduced in [34]. However, in our approach, the coolants are different, and the flow is in direct contact with the LIB surface areas. Such an innovative approach has evidently improved BTMS efficiency and is expected to reduce the weight and cost of the whole system. This new concept is ultimately aimed to introduce a cost-effective technique in a trial to maintain the LIB cells in their optimal temperature range (20 °C – 40 °C). As one will see from the results Section, this has been achieved, in addition to a good temperature uniformity with up to 1 K difference across the module. In what follows, the meshing practice is described.

In this analysis, the numerical simulation is conducted using ANSYS-Fluent CFD software. The convergence is tested for the residuals of all fluid flow governing equations (see Section 2.1). The results are verified with a *mesh independence check* to ensure their reliability. The mesh type is optimised based on the consistency of the LIB module maximum temperature using different types and sizes of mesh elements for both the LIB cells and enclosure (see Figure 3).

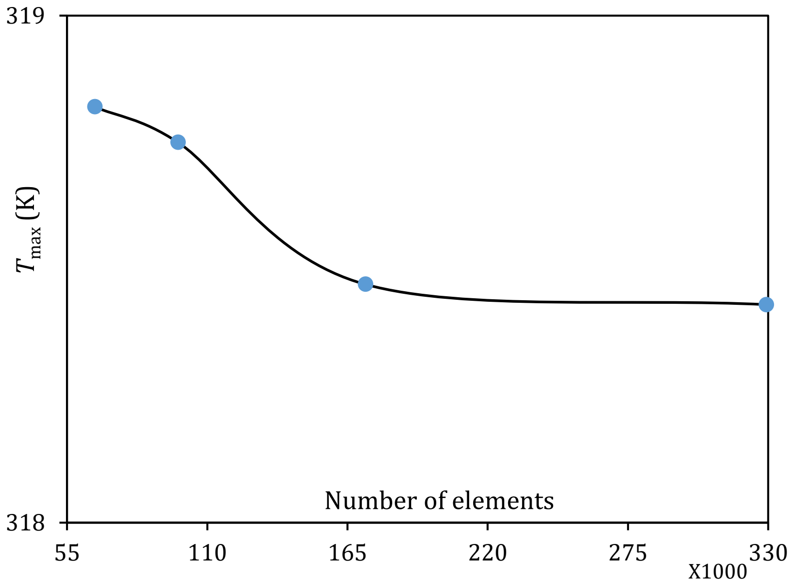

Figure 3. LIB Module maximum temperature versus number of elements, showing grid independence of the battery thermal effect with enclosure.

The enclosure domain is meshed with hexahedron cells. A boundary layer is accounted for with a 1.15 inflation rate and local refinement of prisms cells. The battery module is meshed with four different element categories and various element refinements (in the range: 2 mm – 3.5 mm, and 0.5 mm interval), according to local geometric and flow complexity demands. As can be seen from Figure 3, the LIB module maximum temperature (T_{max}) approaches its consistency at an increased number of elements, up to 329293 elements where T_{max} remains unchanged. Thus, the mesh is considered verified at 329293 elements (element size 2mm). See Figure 4 for further illustration of the geometry meshing.

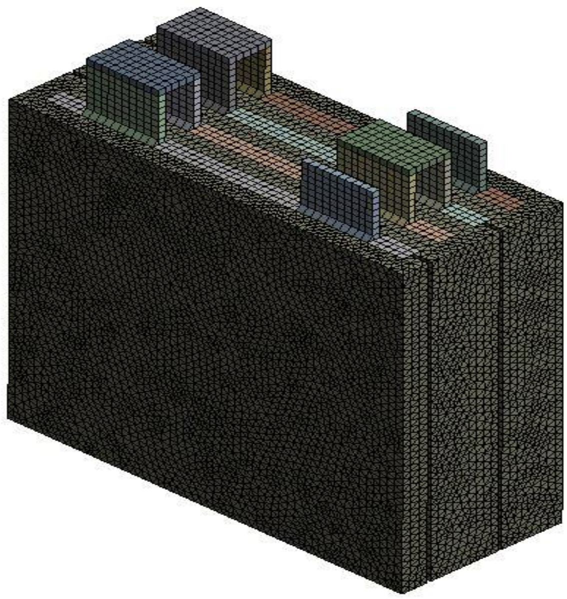

Figure 4. Mesh of the BTMS, using 329293 total elements and 2 mm element size. Uniform structured and tetrahedral mesh types are used for the battery module and fluid domains, respectively.

3. Results

3.1 LIB module without cooling

In this analysis, the LIB module (without cooling) is simulated as the benchmark data to assess each case of the BTMS. The LIB cell temperature distributions are simulated for various discharge rates (1C, 1.5C and 2C) to predict the interaction between the LIB power demand, voltage, and temperature, as shown in Figure 5. The initial temperature of LIB cells was 300 K and voltage was 4.2 V (please refer to Table 3 for the full parameters). The transient simulation of the LIB module is conducted in the range 1C – 2C until complete power discharge, using 1 s time-step.

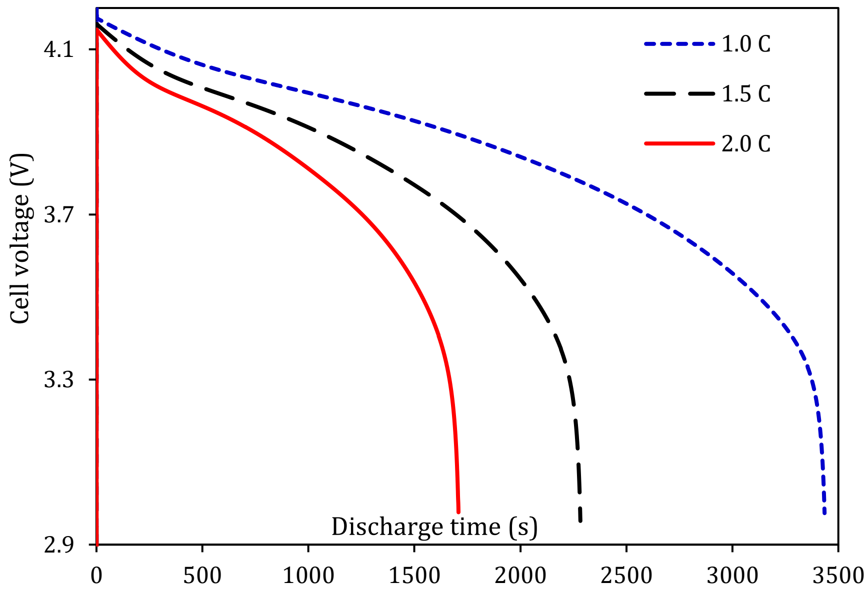

Figure 5. LIB cell voltage versus discharge time at 1C, 1.5C and 2C discharge rates.

As can be seen from Figure 5, the LIB cell power discharge time becomes shorter at high discharge rate (2C), and vice versa at low discharge rate (1C). This is similar to the trend in the literature (e.g. [7]). The LIB module is found to have fully discharged in about 57.25 minutes at 1C, about 38 minutes at 1.5C, and about 28.5 minutes at 2C. The discharge time of the LIB module is slightly shorter than the predicted optimal discharge times of the LIB module (i.e., 60 minutes at 1C, and 30 minutes at 2C). This is attributed to the fact that some energy is dissipated as heat. Note that LIB energy loss into heat can cause as severe damage to its capacity as 95% [8]. To understand the impact of such loss on the temperature rise in the LIB module versus time, this has been illustrated in Figure 6.

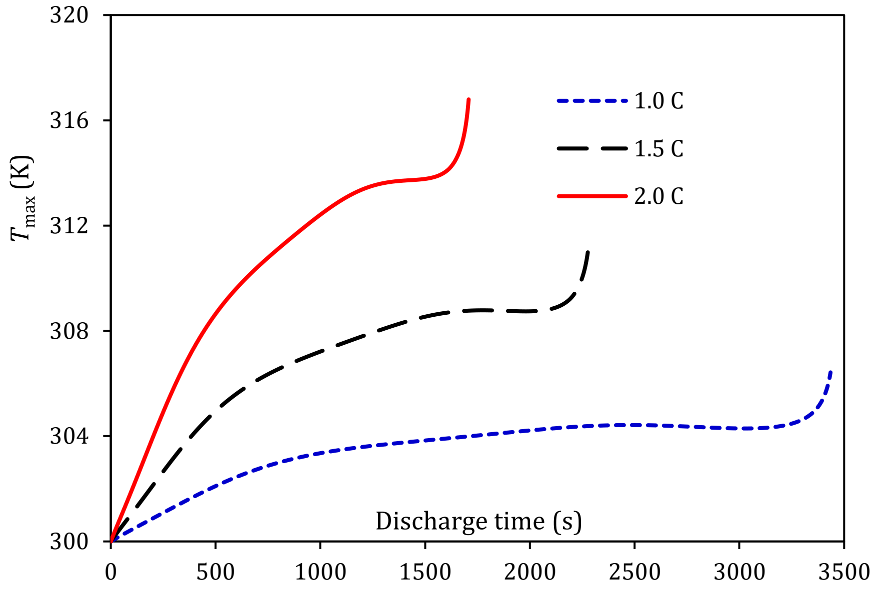

Figure 6. LIB module maximum temperature versus discharge time at 1C, 1.5C and 2C discharge rates.

As can be seen from Figure 6, the increase in the LIB module temperature was always proportional with the discharge time, but it increased more rapidly at higher discharge rates. In the case of 1C rate, the LIB module temperature reached its maximum at about 306.4 K at the full discharge state and 3429 s. In the case of higher discharge rates, the module temperature reached its maximum of 311.4 K at 1.5C and 316.8 K at 2C. One can see that the LIB module temperature exceeded its safe operating temperature. Such a high temperature is a serious problem in practical applications, as it can cause capacity degradation, thermal runaway, and shortened lifespan. The contours of temperature distributions within the LIB module are further investigated for these C-rates (see Figure 10, Appendix A). It is found that the temperature distribution on the LIB module for these cases is non-uniform, which can be a cause of battery thermal degradation and ageing. It turned out from this proof of concept that the BTMS is a necessity to avoid exceeding the optimal temperature and ensure temperature uniformity, which ultimately helps to improve the EV performance and efficiency. In what follows, the BTMS is investigated for three thermal-management coolants.

3.2 Air-cooled system

Air is pumped inside the enclosure to motivate a forced convective heat transfer in direct contact cooling. The air of 298 K is assumed of inlet velocities 0.5 m·s^{-1} and 1 m·s^{-1}. The system is set at three different discharge rates for each inlet velocity; these are 1C, 1.5C and 2C. Therefore, six case studies are investigated for the air-cooled BTMS.

One can see from Figure 7 that the LIB module maximum temperature is decreased to 305.4 K at 1C rate and 0.5 m·s^{-1} inlet velocity (see Table 4 for details). This temperature is found within the recommended LIB range. The air-cooled forced convection has decreased the maximum temperature by 1 K, compared to that of the benchmark results without cooling. At higher discharge rates (1.5C and 2C), the flow has not been sufficient to regulate the LIB module maximum temperature. This can be attributed to the incompetent cooling properties of air (for example, the low specific heat capacity and density). The temperature contours of the system are further illustrated in Figure 11 (Appendix A), which shows poor distribution of temperature across the LIB cells of this module. It has been observed that the temperature of the last two (edge) cells is much higher than those in the middle and other end of the LIB module. It has been noted that a large difference in temperature across the LIB cells can be a cause of their low capacity and high internal resistance. Thus, the air-cooling approach does not conform to the cooling and temperature uniformity requirements of the BTMS.

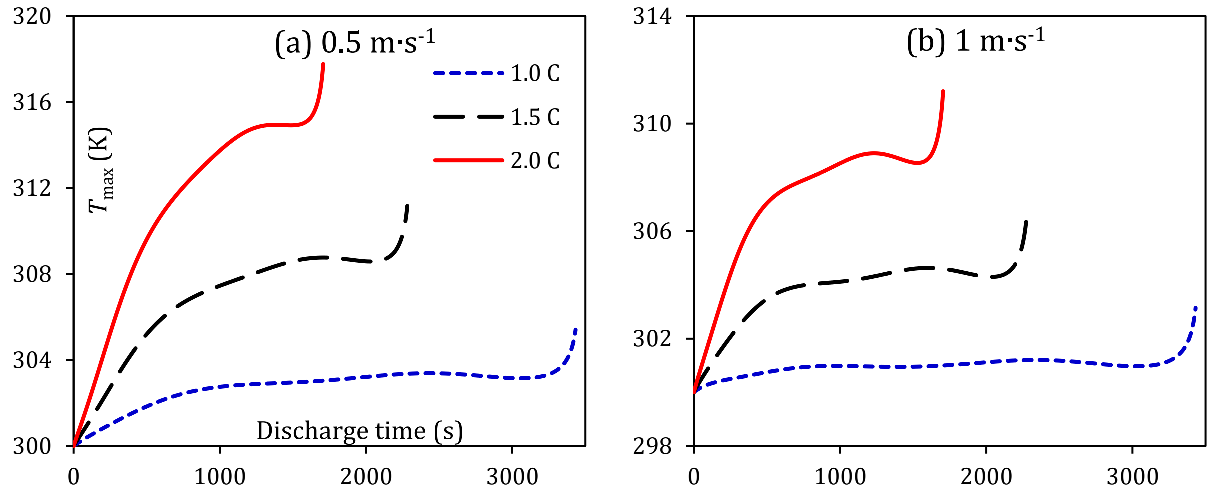

Figure 7. LIB module maximum temperature at air temperature 298 K and inlet velocities: a) 0.5 m·s^{-1} and b) 1 m·s^{-1}, and for discharge rates 1C, 1.5C and 2C.

At 1 m·s^{-1} inlet velocity, and 1C and 1.5C discharge rates, the maximum temperature has been controlled. As can be seen from Table 4, the maximum LIB temperature is decreased within the safe LIB temperature range (for this prismatic LIB, 20 °C – 30 °C [9]) at 1C and 1.5C. The LIB maximum temperature, however, exceeds the optimal range by 3.2 °C at a higher discharge rate (2C). Therefore, this BTMS is still insufficient for controlling the maximum temperature within its safety limit. It neither achieves the temperature uniformity needed for the LIB module at all discharge rates (see Figure 11 for more details).

As can be seen from Figure 7, the LIB module maximum temperature has not been maintained at a constant value with the discharge time, which is consistent with the trends in literature (e.g., [35]). It has, however, not maintained a uniform distribution for the LIB cells at both velocities (0.5 m·s^{-1} and 1 m·s^{-1}). It can be concluded that the forced air-cooling may fulfil the optimal temperature range of LIB in limited cases when reducing the inlet temperature of the air below 293 K and increasing the inlet velocity above 1 1 m·s^{-1}, which are not practical and inconvenient cases in general applications.

Table 4. LIB module and individual cell temperature ranges in K at air inlet velocities 0.5 m·s^{-1} and 1 m·s^{-1}.

LIB component	1C		1.5C		2C	
	T_{max} K	T_{min} K	T_{max} K	T_{min} K	T_{max} K	T_{min} K
Inlet velocity = 0.5 m·s^{-1}						
Module range	305.4	301.7	311.2	304.4	317.8	307.5
Cell1	302.2	301.8	305.2	304.5	308.7	307.7
Cell2	303.4	302.3	307.4	305.5	312.2	309.4
Cell3	304.5	303.5	309.5	307.8	315.3	312.8
Cell4	305.4	304.4	311.2	309.5	317.8	315.5
Inlet velocity = 1 m·s^{-1}						
Module range	303.1	300.8	306.8	302.6	311.2	304.8
Cell1	301.1	300.8	303.2	302.7	305.6	304.9
Cell2	301.8	301.1	304.4	303.2	307.4	305.7
Cell3	302.5	301.8	305.7	304.5	309.5	307.8
Cell4	303.1	302.4	306.8	305.7	311.2	309.6

3.3 3M-Novec cooled system

Three different inlet velocities were considered in 3M-Novec 7200 coolant namely 0.1 m·s^{-1}, 0.5 m·s^{-1}, and 1.0 m·s^{-1}. Each inlet velocity was tested at three discharge rates, 1C, 1.5C, and 2C. Table 5 shows simulation results of inlet velocities against the discharge rates. 3-M Novec 7200 coolant was able to keep the LIB module maximum temperature consistently for every inlet velocity and discharge rate as well as the homogenous surface temperature distribution between LIB cells.

Table 5. LIB module and cell temperatures in K using 3M-Novec 7200 coolant at three inlet velocities (0.1 m·s^{-1}, 0.5 m·s^{-1} and 1 m·s^{-1}) and three different discharge rates.

LIB component	1C		1.5C		2C	
	T_{max}	T_{min}	T_{max}	T_{min}	T_{max}	T_{min}
Inlet velocity = 0.1 m·s^{-1}						
Module range	298.6	298.4	299.0	298.6	299.4	298.9
Cell1	298.6	298.4	298.9	298.6	299.4	298.9

Cell2	298.6	298.4	299.0	298.6	299.3	298.9
Cell3	298.6	298.4	299.0	298.7	299.4	298.9
Cell4	298.6	298.4	299.0	298.7	299.4	299.0
Inlet velocity = 0.5 $m \cdot s^{-1}$						
Module range	298.3	298.1	298.4	298.1	298.5	298.2
Cell1	298.2	298.1	298.4	298.2	298.5	298.2
Cell2	298.2	298.1	298.3	298.1	298.5	298.2
Cell3	298.2	298.1	298.3	298.2	298.5	298.2
Cell4	298.3	298.1	298.3	298.2	298.5	298.2
Inlet velocity = 1.0 $m \cdot s^{-1}$						
Module range	298.2	298.1	298.3	298.1	298.3	298.1
Cell1	298.5	298.1	298.2	298.1	298.3	298.1
Cell2	298.1	298.1	298.2	298.1	298.3	298.1
Cell3	298.1	298.1	298.2	298.1	298.3	298.1
Cell4	298.2	298.1	298.3	298.1	298.3	298.1

In Figure 8, the LIB module maximum temperature at 0.1 $m \cdot s^{-1}$ and discharge rate of 2C was slightly increased by 1.4 K, which was only an 8 % increment compared to the benchmark coolant at the same discharge rate. This increment has no significant impact on the LIB module performance and efficiency. Also, the maximum surface temperature distribution consistency across LIB cells was kept below 0.5 K for all discharge rates, as shown in Figure 12 (Appendix A). When the inlet velocities were increased to 0.5 $m \cdot s^{-1}$ and 1.0 $m \cdot s^{-1}$, the LIB module maximum temperature was not considerably affected by increasing the discharge rate. The consistency of surface temperature distribution was slightly better than inlet velocity of 0.1 $m \cdot s^{-1}$, at less than 0.3 K. It has primarily contributed to reducing the LIB module temperature and maintaining its uniformity.

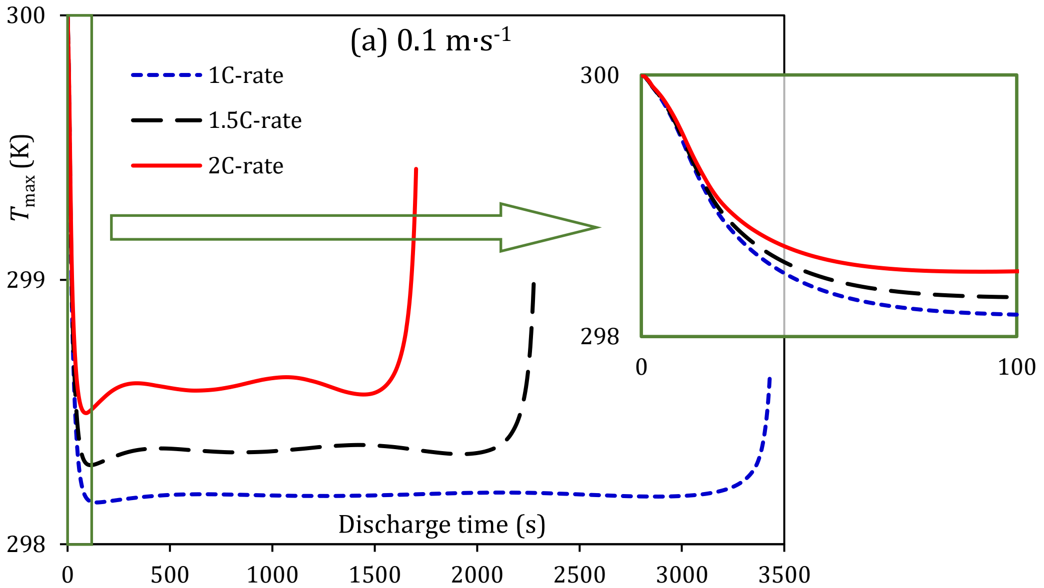

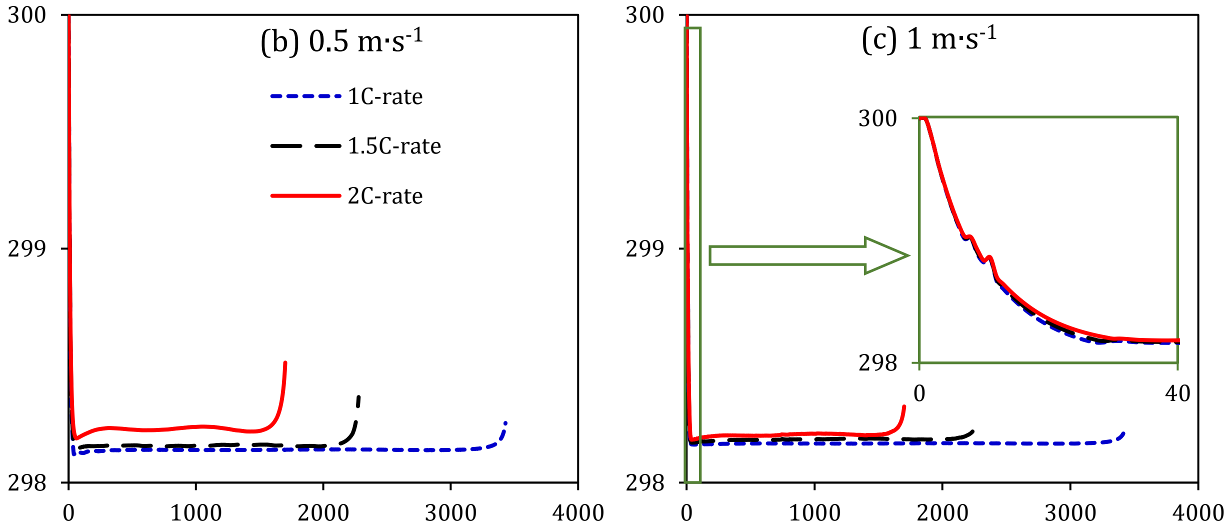

Figure 8. LIB module maximum temperature at discharge rates of 1C, 1.5C, 2C, and 3M-Novec 7200 coolant inlet velocities: a) 0.1 $m{\cdot}s^{-1}$, b) 0.5 $m{\cdot}s^{-1}$; c) 1.0 $m{\cdot}s^{-1}$. The maximum and minimum velocities of these cases are shown in Table 5.

3.4 N-heptane cooled system

In this section, the n-heptane cooling performance was studied using dominating inlet velocity. This cooling method can reduce the vehicle weight without relying on heavy coolants such as 3M-Novec 7200 and subsequently improve the energy consumption and CO_2 emission. However, n-heptane coolant should not exceed its flashpoint temperature if it comes in direct contact with the LIB cells to avoid fire. As discussed earlier, the inlet velocity, discharge rate, and inlet temperature have significant impacts on the thermal management of the LIB module. Hence, the same inlet velocities as in the case of 3M Novec coolant were used to verify the predicted performance of the n-heptane coolant. Figure 9 shows the temperature trends based on three inlet velocities and three discharge rates. When the inlet velocity of n-heptane coolant was set at 0.1 m·s-1, the LIB module maximum temperature behaviour was very similar to that of 3M Novec coolant with up to 0.1% error, as shown in Table 6.

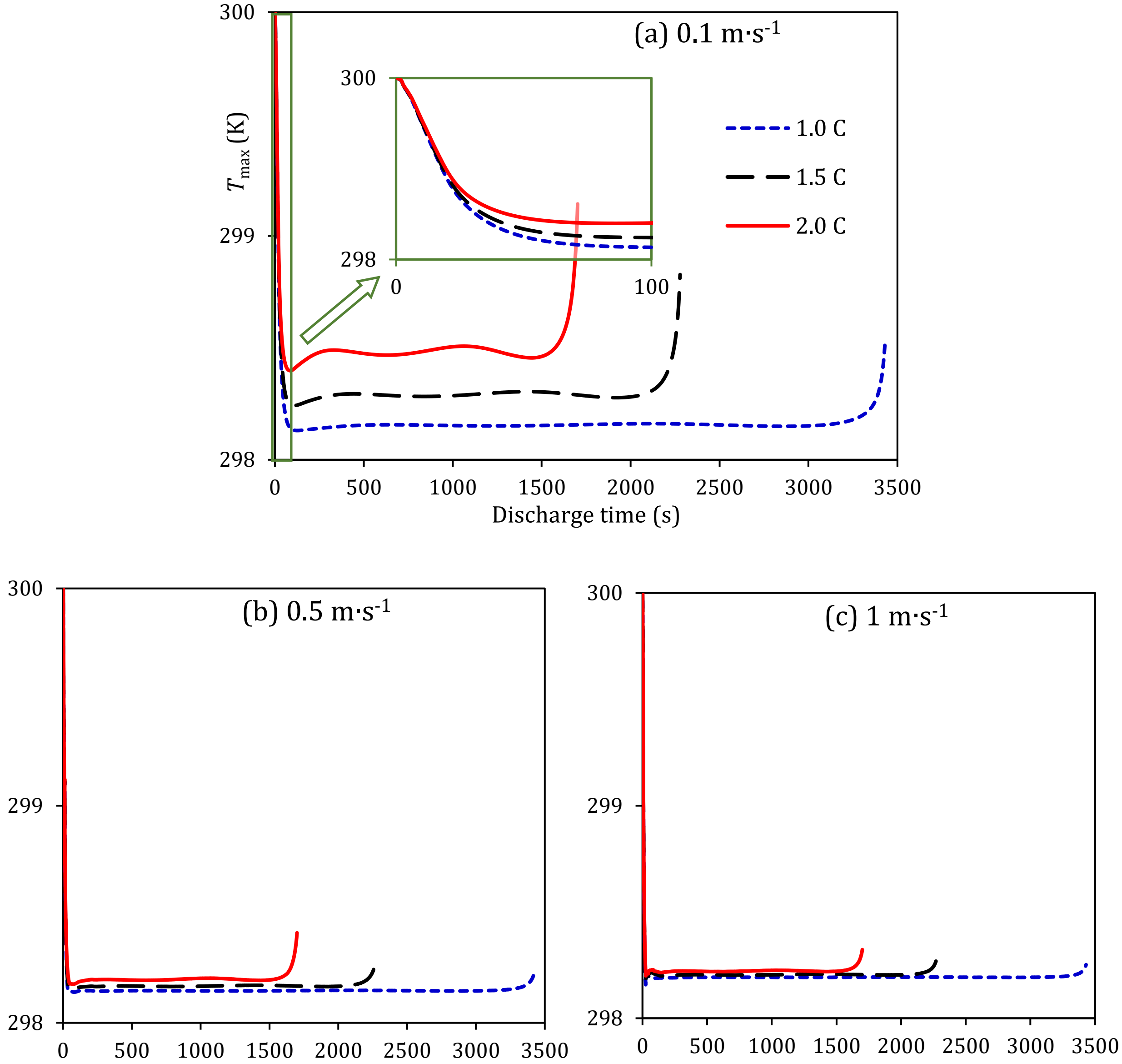

Figure 9. LIB module maximum temperature at discharge rates of 1C, 1.5C, 2C, and n-heptane coolant inlet velocities: (a) 0.1 m·s^{-1}; (b) 0.5 m·s^{-1}, (c) 1.0 m·s^{-1}. The maximum and minimum velocities of these cases are shown in Table 6.

Table 6. LIB module and cell temperatures using n-heptane coolant at three inlet velocities (0.1 m·s^{-1}, 0.5 m·s^{-1} and 1 m·s^{-1}) and three discharge rates.

LIB component	1C		1.5C		2C	
	T_{max}	T_{min}	T_{max}	T_{min}	T_{max}	T_{min}
Inlet velocity = 0.1 m·s^{-1}						

Module maximum	298.5	298.3	298.8	298.5	299.1	298.7
Cell1	298.5	298.3	298.8	298.5	299.0	298.7
Cell2	298.5	298.3	298.8	298.5	299.0	298.7
Cell3	298.5	298.3	298.8	298.5	299.1	298.7
Cell4	298.5	298.3	298.8	298.6	299.1	298.8
Inlet velocity = 0.5 $m \cdot s^{-1}$						
Module maximum	298.3	298.1	298.3	298.1	298.4	298.2
Cell1	298.2	298.1	298.3	298.1	298.4	298.2
Cell2	298.2	298.1	298.3	298.1	298.4	298.2
Cell3	298.2	298.1	298.3	298.1	298.4	298.2
Cell4	298.3	298.1	298.3	298.1	298.4	298.2
Inlet velocity = 1.0 $m \cdot s^{-1}$						
Module maximum	298.3	298.0	298.3	298.1	298.3	298.1
Cell1	298.1	298.0	298.2	298.1	298.3	298.1
Cell2	298.1	298.0	298.2	298.1	298.3	298.1
Cell3	298.1	298.1	298.2	298.1	298.3	298.1
Cell4	298.3	298.1	298.3	298.1	298.3	298.1

Using n-heptane as a coolant at discharge rates 1C and 2C is found to have reduced the LIB module maximum temperature by 17.9 K and 7.9 K, respectively, compared with those of benchmark results. The surface temperature distribution also was kept homogenous across three discharge rates with a maximum difference of 0.4 K as can be observed in Figure 9. Increasing the inlet velocity has also reduced the LIB module maximum temperature. For instance, the temperature reduction at inlet velocities of 0.5 $m \cdot s^{-1}$ and 1.0 $m \cdot s^{-1}$, compared to 0.1 $m \cdot s^{-1}$ at 2C was 0.7 K and 0.8 K respectively. At the inlet velocity 0.1 $m \cdot s^{-1}$, the LIB module maximum temperature operated at a linear trend at almost discharge time at 1C. However, at 1.5C and 2C, the temperature trends fluctuated until they were fully depleted and raised the temperature due to higher internal resistance at low SOC. The differences of temperature 0.5 $m \cdot s^{-1}$and 1.0 $m \cdot s^{-1}$, and three discharge rates were small, where n-heptane coolant managed to cool down the LIB module effective at low SOC, a reduction by 18.6 K and 18.7 K respectively compared to the air cooling results.

3.5 Comparative analysis

The hydrocarbon fuel of n-heptane is compared to the most common cooling strategies to showcase a worthwhile cooling option of BTMS in HEV (see Appendix A for illustration). The simulation results exhibit that both (3M Novec and n-heptane) liquid coolants are far better than the air-cooled BTMS. Using liquid coolants, the LIB module maximum temperature was kept and regulated below 313 K. The trend of temperature increased in the air-cooled forced convection almost in logarithmic growth, which was slower than the linear rise of the benchmark model temperature. This technique showed a good improvement compared to the benchmark results, but it also had a drawback. The air did not cool down the LIB module sufficiently quickly at low velocities, in the assumption of passive cooling to avoid losing energy to the fan. In passive cooling, e.g. using only natural convection, no energy is consumed and the LIB module is aimed to be maintained below its maximum safety temperature. This arrangement reduces the amount of energy used in the system and increases the vehicle range. This approach, however, may not be a feasible option in an air-cooled BTMS because air cannot drastically change the temperature of the LIB module at moderate velocities and may require high speed fans.

Similarly to n-heptane, using 3M Novec 7200 coolant made the LIB module maximum temperature more controllable, where the temperature did not fluctuate drastically at every inlet velocity and discharge rate. This feature makes both coolants very useful and effective solutions as it does not allow the LIB module maximum temperature to go above the coolant temperature for a long period of time. They both managed to maintain the LIB module maximum temperature at a constant level for a long period. Both liquid coolants had almost identical LIB module maximum temperature curves. However, n-heptane was slightly better at exchanging heat as can be seen in the first 500 s of the discharging time, and it had relatively the lowest LIB module maximum temperature. Additionally, n-heptane has an advantage over the 3M Novec 7200 coolant in terms of low density, which can contribute to the overall vehicle light-weighting and energy reserve. These results show that n-heptane can be a doable coolant for HEV BTMS thus supporting the hypothesis of this work. See Figure 14 for further illustration of these findings.

In practice, using liquid coolants can demand higher pumping power than that needed for high-speed air fans. To minimise the system exergy, it is suggested that the LIB module can be passively cooled until it reaches a temperature close to a safeguard value (approximately 313 K). Once the safeguard temperature is reached, the fluid is pumped through the system to cool it down, back to normal. This method can reduce vehicle energy consumption and CO_2 emission.

4. Conclusions

The importance of Battery Thermal Management Systems (BTMS) was successfully validated using the commercial CFD tool of ANSYS-Fluent. The benchmark simulation results showed an almost linear increase in temperature with the increase in discharge time. Such phenomenon was more significant at higher discharge rates, which led to a heated LIB module at a very high heating rate. At a higher discharge rate, the LIB module maximum temperature reached the allowable maximum temperature that can lead to thermal runaway, which required an effective BTMS to maintain the temperature within the optimum operating temperature. The proposed n-heptane coolant provided a significant decrease in the LIB module maximum temperature compared to other cooling strategies. The ability of n-heptane coolant to keep the LIB module maximum temperature constant for an extended period making it an effective solution for BTMS. The relatively low density of n-heptane and zero weight of liquid-coolants can help the overall vehicle light-weighting and significantly improve energy consumption. n-heptane would be a viable option to use in the HEV BTMS and this hypothesis has been supported with the results obtained from CFD. N-heptane BTMS managed to minimize the impact of discharge rates between 1C and 2C on the maximum module temperatures for all inlet velocities. At the lowest inlet velocity of 0.1 $m \cdot s^{-1}$, the LIB module maximum temperatures at 1C, 1.5C, 2C were 298.5 K, 299.0 K, and 299.1 K respectively. For a higher inlet velocity, 1.0 $m \cdot s^{-1}$, the maximum LIB module maximum temperatures were kept constant at 298.3 K for all discharge rates. Also, n-heptane reduced the LIB module maximum temperature by 18.6 K at 0.5 $m \cdot s^{-1}$ and 18.7 K at 1 $m \cdot s^{-1}$ compared to without cooling strategy. Another important aspect of n-heptane was that the temperature gradients between LIB cells were kept below 1 K that can prevent LIB degradation over time.

References

[1] Liu J, Li H, Li W, Shi J, Wang H, Chen J. Thermal characteristics of power battery pack with liquid-based thermal management. Applied Thermal Engineering 2020;164:114421. https://doi.org/10.1016/j.applthermaleng.2019.114421.

[2] Zhang F, Hu X, Langari R, Wang L, Cui Y, Pang H. Adaptive energy management in automated hybrid electric vehicles with flexible torque request. Energy 2021;214:118873. https://doi.org/10.1016/j.energy.2020.118873.

[3] Xia G, Cao L, Bi G. A review on battery thermal management in electric vehicle application. Journal of Power Sources 2017;367:90–105. https://doi.org/10.1016/j.jpowsour.2017.09.046.

[4] Fuel types of new passenger cars. European Automobile Manufacturers' Association (ACEA) 2021. https://www.acea.be/statistics/tag/category/share-of-diesel-in-new-passenger-cars (accessed April 8, 2021).

[5] Ding Y, Cano ZP, Yu A, Lu J, Chen Z. Automotive Li-Ion Batteries: Current Status and Future Perspectives. Electrochem Energ Rev 2019;2:1–28. https://doi.org/10.1007/s41918-018-0022-z.

[6] Bisschop R, Willstrand O, Rosengren M. Handling Lithium-Ion Batteries in Electric Vehicles: Preventing and Recovering from Hazardous Events. Fire Technol 2020;56:2671–94. https://doi.org/10.1007/s10694-020-01038-1.

[7] Alipour M, Esen E, Varzeghani AR, Kizilel R. Performance of high capacity Li-ion pouch cells over wide range of operating temperatures and discharge rates. Journal of Electroanalytical Chemistry 2020;860:113903. https://doi.org/10.1016/j.jelechem.2020.113903.

[8] Spitthoff L, Shearing PR, Burheim OS. Temperature, Ageing and Thermal Management of Lithium-Ion Batteries. Energies 2021;14:1248. https://doi.org/10.3390/en14051248.

[9] Liang L, Zhao Y, Diao Y, Ren R, Zhang L, Wang G. Optimum cooling surface for prismatic lithium battery with metal shell based on anisotropic thermal conductivity and dimensions. Journal of Power Sources 2021;506:230182. https://doi.org/10.1016/j.jpowsour.2021.230182.

[10] Al Qubeissi M, El-kharouf A, Serhad Soyhan H, editors. Renewable Energy - Resources, Challenges and Applications. IntechOpen; 2020. https://doi.org/10.5772/intechopen.81765.

[11] Al Qubeissi M, editor. Biofuels - Challenges and opportunities. IntechOpen; 2019. https://doi.org/10.5772/intechopen.76490.

[12] Liu C, Lin J, Cao H, Zhang Y, Sun Z. Recycling of spent lithium-ion batteries in view of lithium recovery: A critical review. Journal of Cleaner Production 2019;228:801–13. https://doi.org/10.1016/j.jclepro.2019.04.304.

[13] Akinlabi AAH, Solyali D. Configuration, design, and optimization of air-cooled battery thermal management system for electric vehicles: A review. Renewable and Sustainable Energy Reviews 2020;125:109815. https://doi.org/10.1016/j.rser.2020.109815.

[14] Jilte R, Afzal A, Panchal S. A novel battery thermal management system using nano-enhanced phase change materials. Energy 2021;219:119564. https://doi.org/10.1016/j.energy.2020.119564.

[15] An Z, Jia L, Ding Y, Dang C, Li X. A review on lithium-ion power battery thermal management technologies and thermal safety. J Therm Sci 2017;26:391–412. https://doi.org/10.1007/s11630-017-0955-2.

[16] 3M™ Novec™ 7000 Engineered Fluid. 3M Science Applied to Life 2020. https://www.3m.com/3M/en_US/company-us/SDS-search/ (accessed July 28, 2021).

[17] van Gils RW, Danilov D, Notten PHL, Speetjens MFM, Nijmeijer H. Battery thermal management by boiling heat-transfer. Energy Conversion and Management 2014;79:9–17. https://doi.org/10.1016/j.enconman.2013.12.006.

[18] Rybdylova O, Al Qubeissi M, Braun M, Crua C, Manin J, Pickett LM, et al. A model for droplet heating and its implementation into ANSYS Fluent. International Communications in Heat and Mass Transfer 2016. https://doi.org/10.1016/j.icheatmasstransfer.2016.05.032.

[19] Bibin C, Vijayaram M, Suriya V, Sai Ganesh R, Soundarraj S. A review on thermal issues in Li-ion battery and recent advancements in battery thermal management system. Materials Today: Proceedings 2020;33:116–28. https://doi.org/10.1016/j.matpr.2020.03.317.

[20] Kim J, Oh J, Lee H. Review on battery thermal management system for electric vehicles. Applied Thermal Engineering 2019;149:192–212. https://doi.org/10.1016/j.applthermaleng.2018.12.020.

[21] Zhao G, Wang X, Negnevitsky M, Zhang H. A review of air-cooling battery thermal management systems for electric and hybrid electric vehicles. Journal of Power Sources 2021;501:230001. https://doi.org/10.1016/j.jpowsour.2021.230001.

[22] Tan X, Lyu P, Fan Y, Rao J, Ouyang K. Numerical investigation of the direct liquid cooling of a fast-charging lithium-ion battery pack in hydrofluoroether. Applied Thermal Engineering 2021;196:117279. https://doi.org/10.1016/j.applthermaleng.2021.117279.

[23] Dubey P, Pulugundla G, Srouji AK. Direct Comparison of Immersion and Cold-Plate Based Cooling for Automotive Li-Ion Battery Modules. Energies 2021;14:1259. https://doi.org/10.3390/en14051259.

[24] Al Qubeissi M. Predictions of droplet heating and evaporation: an application to biodiesel, diesel, gasoline and blended fuels. Applied Thermal Engineering 2018;136:260–7. https://doi.org/10.1016/j.applthermaleng.2018.03.010.

[25] Al Qubeissi M, Sazhin SS, Turner J, Begg S, Crua C, Heikal MR. Modelling of gasoline fuel droplets heating and evaporation. Fuel 2015;159:373–84. https://doi.org/10.1016/j.fuel.2015.06.028.

[26] Ho V-T, Chang K, Lee SW, Kim SH. Transient Thermal Analysis of a Li-Ion Battery Module for Electric Cars Based on Various Cooling Fan Arrangements. Energies 2020;13:2387. https://doi.org/10.3390/en13092387.

[27] Zhang H, Li C, Zhang R, Lin Y, Fang H. Thermal analysis of a 6s4p Lithium-ion battery pack cooled by cold plates based on a multi-domain modeling framework. Applied Thermal Engineering 2020;173:115216. https://doi.org/10.1016/j.applthermaleng.2020.115216.

[28] Al Qubeissi M. Proposing a Numerical Solution for the 3D Heat Conduction Equation, IEEE; 2012, p. 144–9. https://doi.org/10.1109/AMS.2012.10.

[29] Amiribavandpour P, Shen W, Mu D, Kapoor A. An improved theoretical electrochemical-thermal modelling of lithium-ion battery packs in electric vehicles. Journal of Power Sources 2015;284:328–38. https://doi.org/10.1016/j.jpowsour.2015.03.022.

[30] Sarkar J, Bhattacharyya S. Operating characteristics of transcritical CO2 heat pump for simultaneous water cooling and heating. Archives of Thermodynamics 2011;33:23–40. https://doi.org/10.2478/v10173-012-0026-8.

[31] Al-Damook M, Obaid ZAH, Al Qubeissi M, Dixon-Hardy D, Cottom J, Heggs PJ. CFD modeling and performance evaluation of multipass solar air heaters. Numerical Heat Transfer, Part A: Applications 2019:1–27. https://doi.org/10.1080/10407782.2019.1637228.

[32] Panchal S, Khasow R, Dincer I, Agelin-Chaab M, Fraser R, Fowler M. Thermal design and simulation of mini-channel cold plate for water cooled large sized prismatic lithium-ion battery. Applied Thermal Engineering 2017;122:80–90. https://doi.org/10.1016/j.applthermaleng.2017.05.010.

[33] Wang Y-F, Wu J-T. Thermal performance predictions for an HFE-7000 direct flow boiling cooled battery thermal management system for electric vehicles. Energy Conversion and Management 2020;207:112569. https://doi.org/10.1016/j.enconman.2020.112569.

[34] Suresh Patil M, Seo J-H, Lee M-Y. A novel dielectric fluid immersion cooling technology for Li-ion battery thermal management. Energy Conversion and Management 2021;229:113715. https://doi.org/10.1016/j.enconman.2020.113715.

[35] Bharathraj S, Kaushik A, Adiga SP, Kolake SM, Song T, Sung Y. Accessing the current limits in lithium ion batteries: Analysis of propensity for unexpected power loss as a function of depth of discharge, temperature and pulse duration. Journal of Power Sources 2021;494:229723. https://doi.org/10.1016/j.jpowsour.2021.229723.

APPENDIX A. Temperature distribution

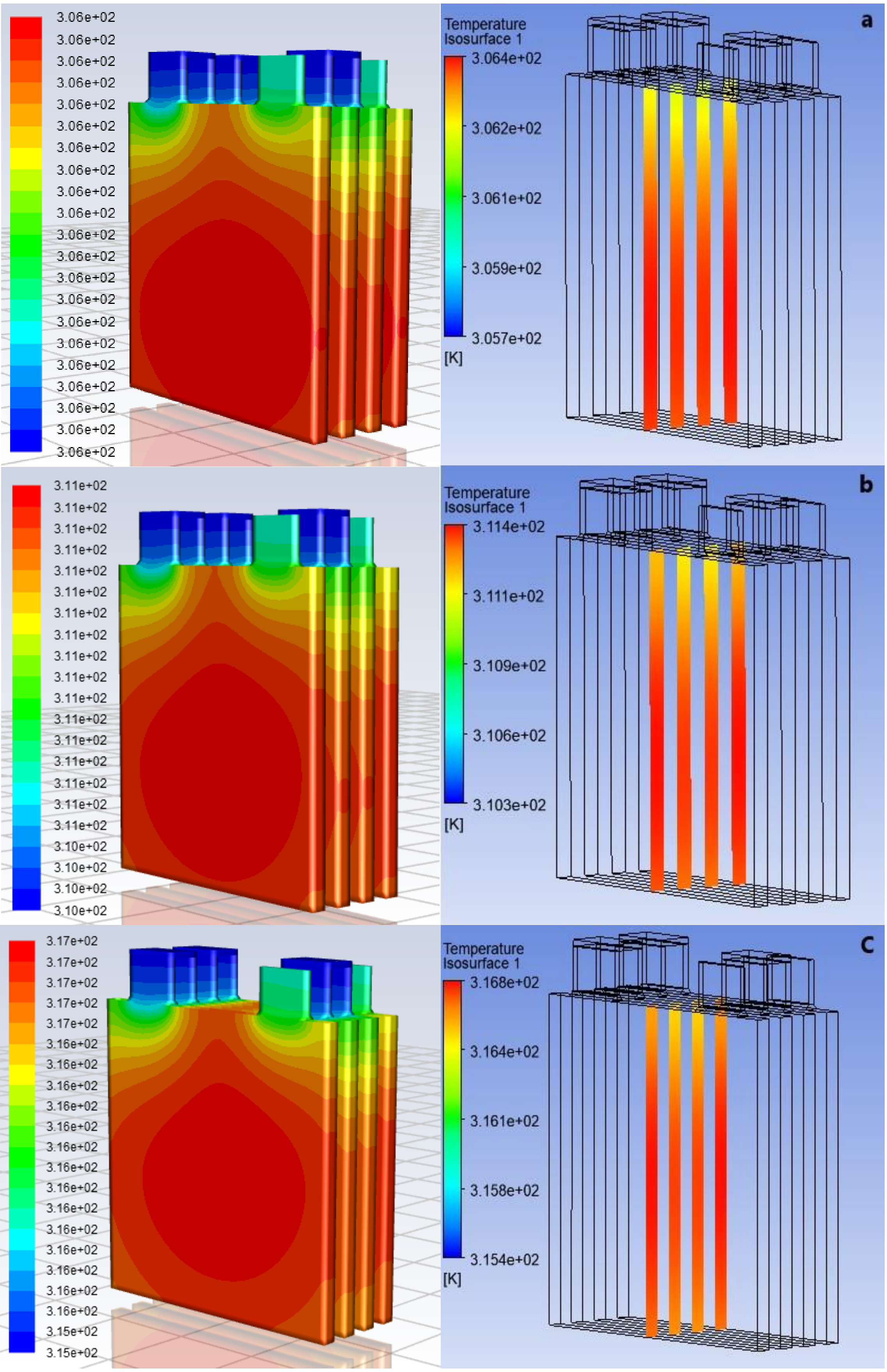

Figure 10. Temperature contours of the battery module without cooling at discharge rates 1 (a), 1.5 (b) and 2 (c) C-rates.

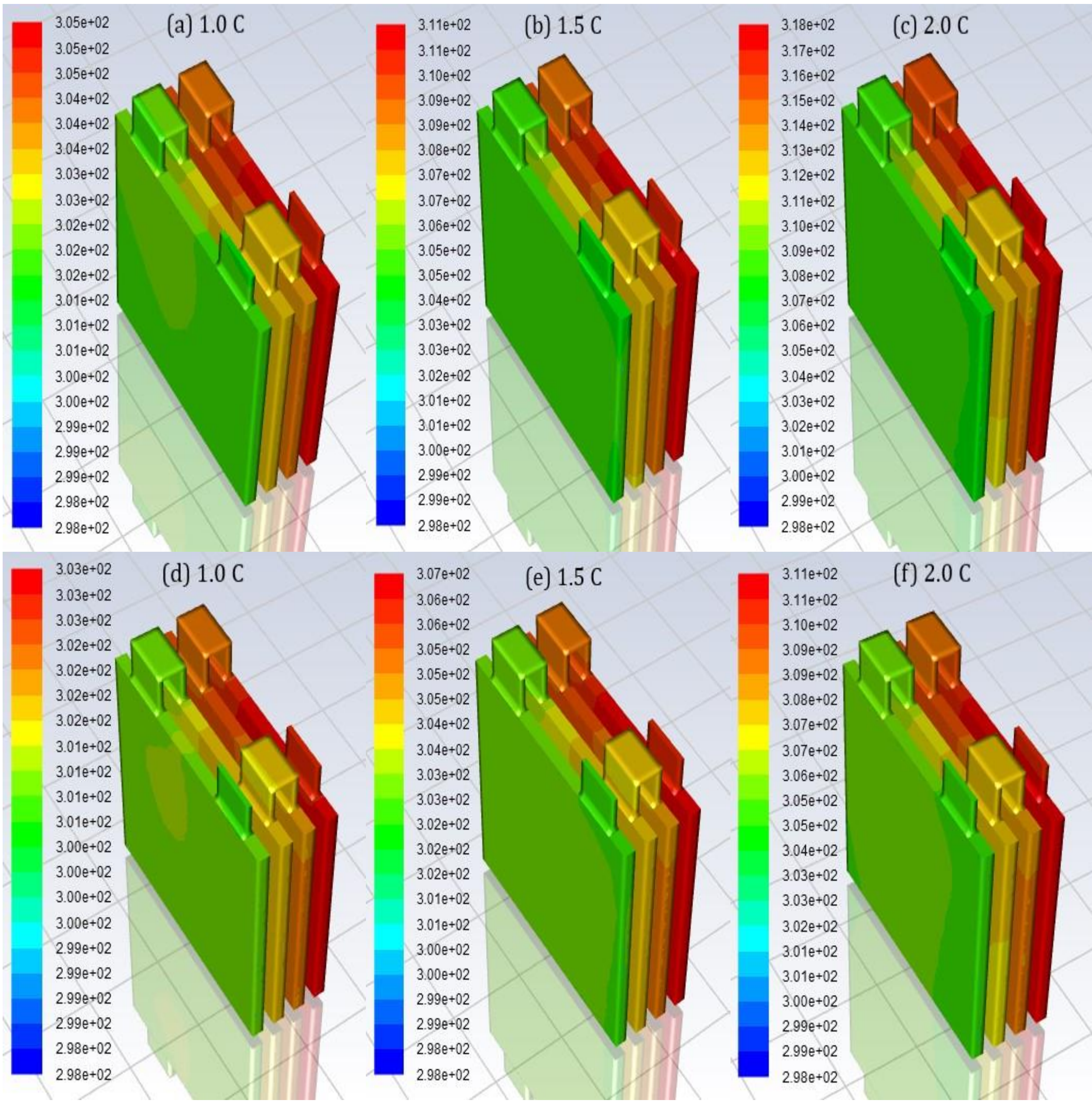

Figure 11. Temperature contours of the battery module using air as coolant at 1C (a and d), 1.5C (b and e) and 2C (c and f) discharge rates, and at 0.5 m·s^{-1} (a, b and c) and 1 m·s^{-1} (d, e and f) inlet velocities.

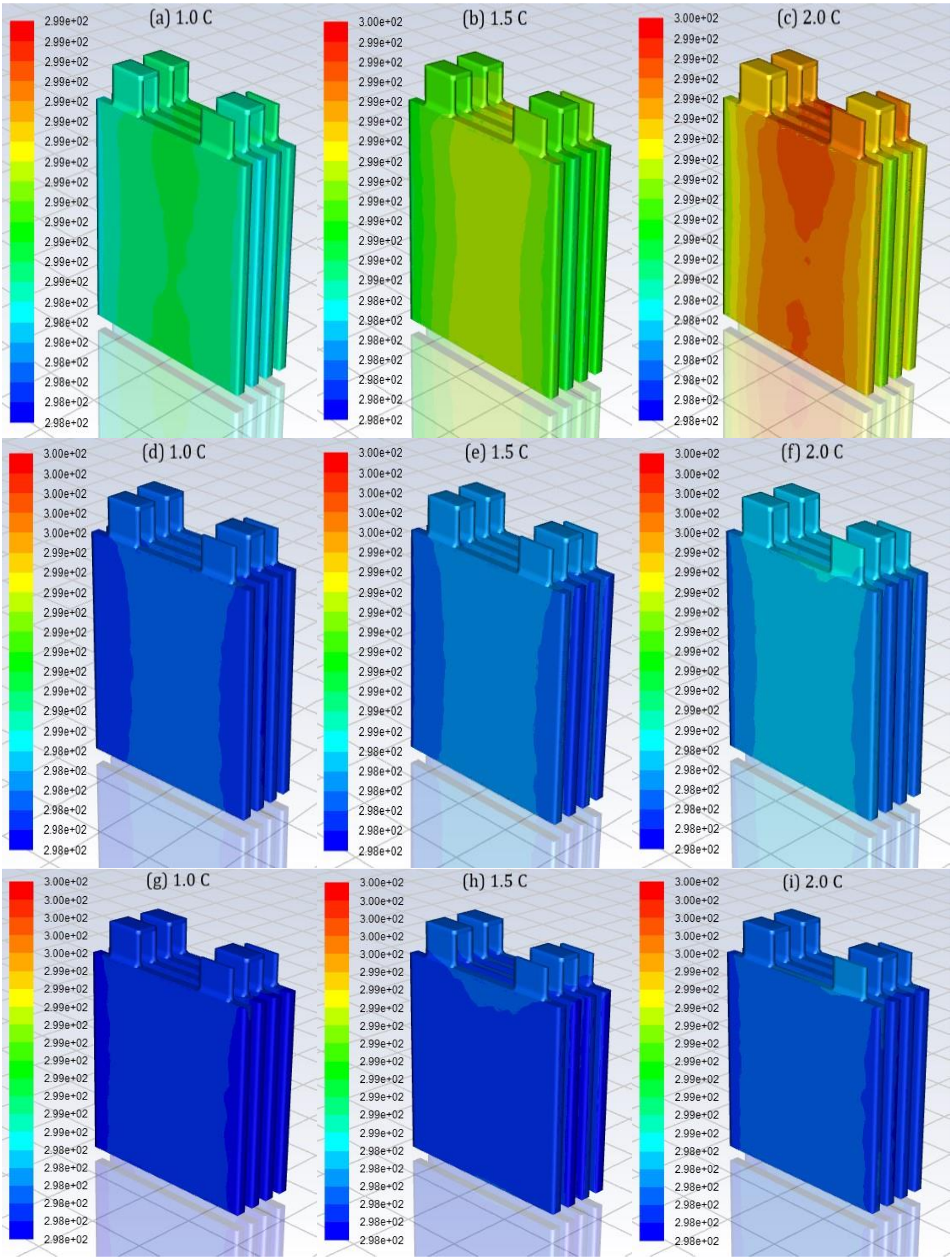

Figure 12. Temperature contours of the battery module using 3M-Novec as coolant at 1C (a, d and g), 1.5C (b, e and h) and 2C (c, f and i) discharge rates, and at 0.1 $m\cdot s^{-1}$ (a, b and c), 0.5 $m\cdot s^{-1}$ (d, e and f) and 1 $m\cdot s^{-1}$ (g, h and i) inlet velocities.

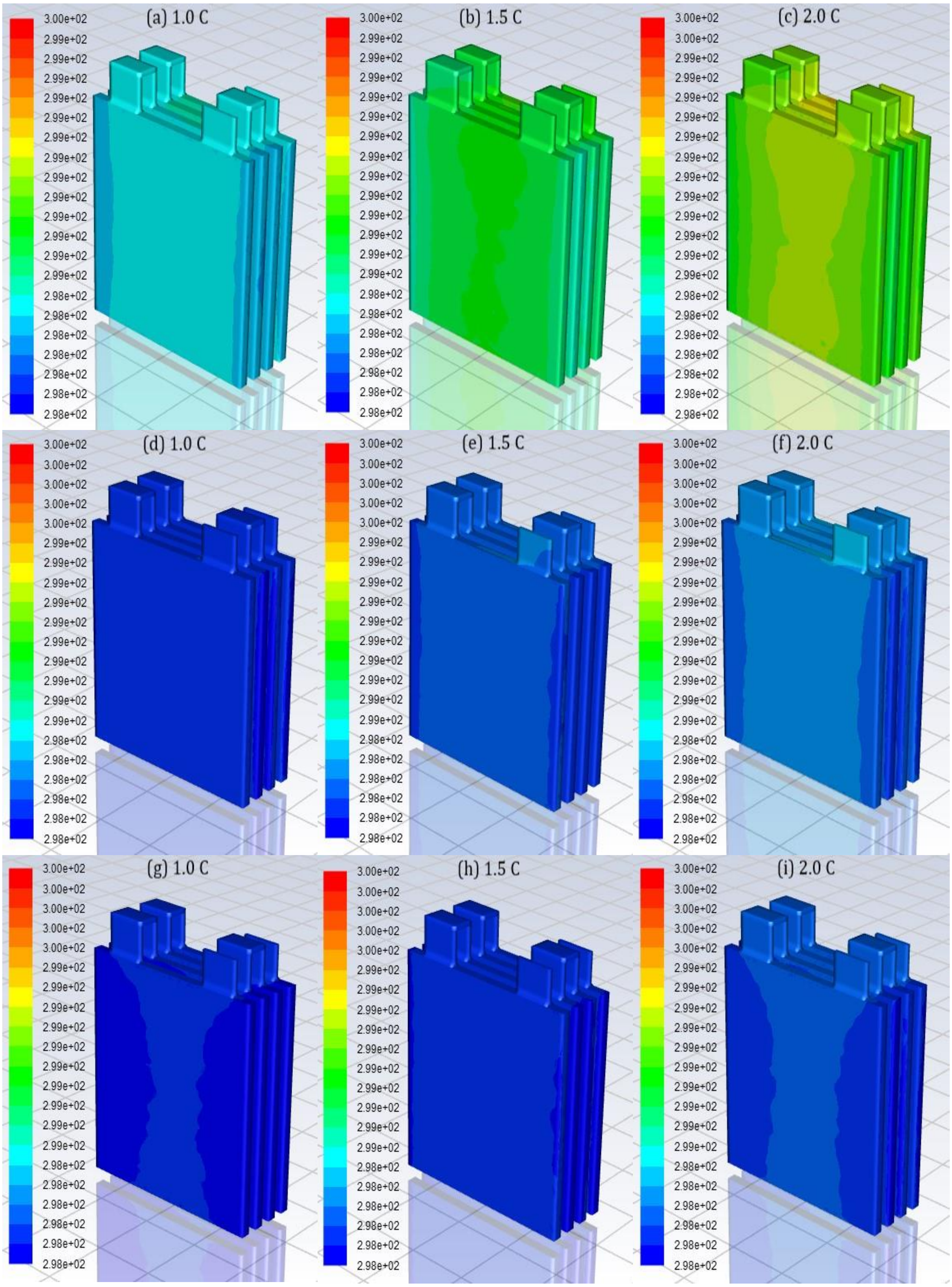

Figure 13. Temperature contours of the battery module using n-heptane as coolant at 1C (a, d and g), 1.5C (b, e and h) and 2C (c, f and i) discharge rates, and at 0.1 $m \cdot s^{-1}$ (a, b and c), 0.5 $m \cdot s^{-1}$ (d, e and f) and 1 $m \cdot s^{-1}$ (g, h and i) inlet velocities.

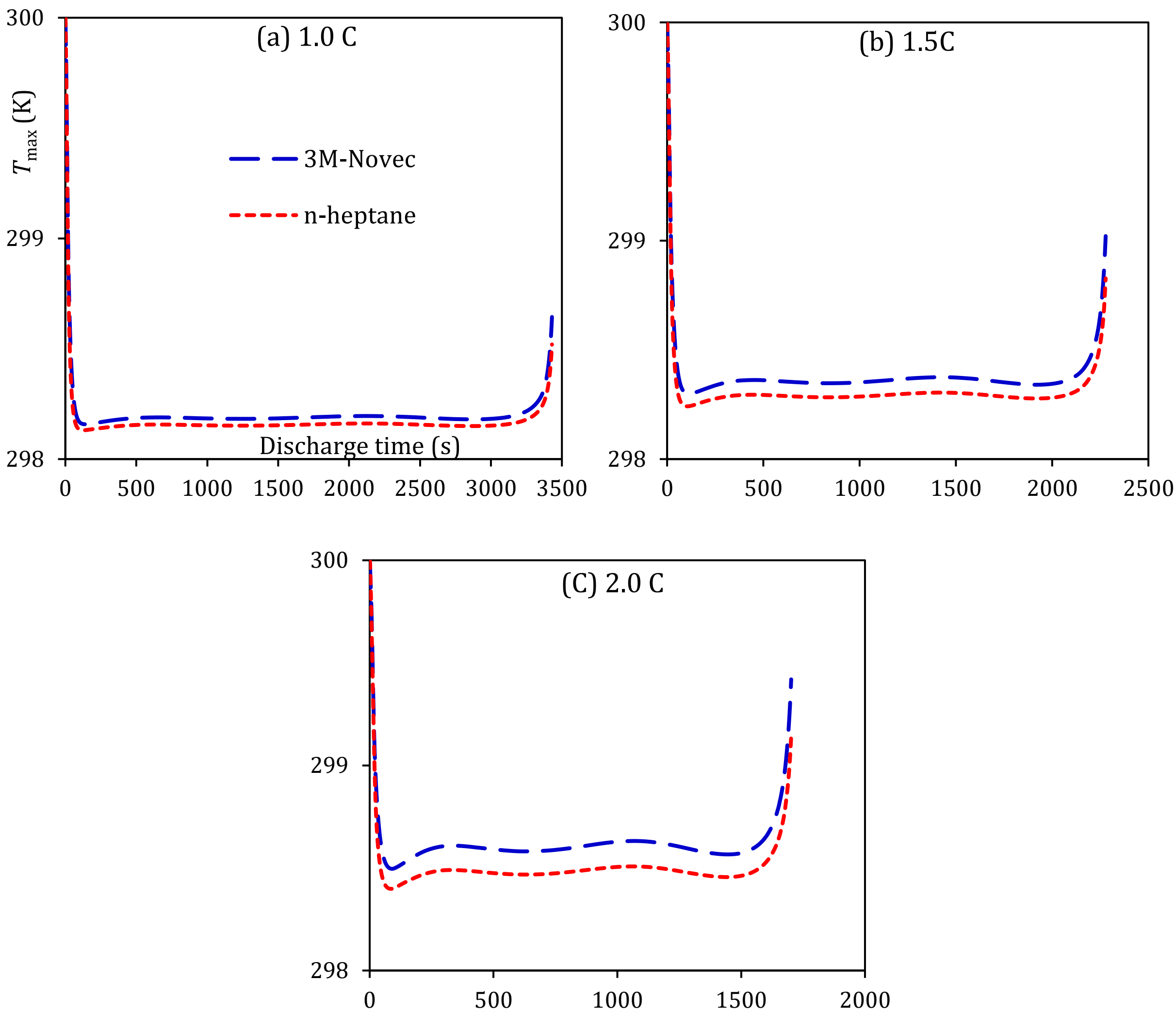

Figure 14. Module maximum temperature versus discharge time at 0.1 m·s^{-1} inlet velocity and (a) 1C, (b) 1.5C and (c) 2C discharge rates, using 3M-Novec 7200 and n-heptane as coolants.

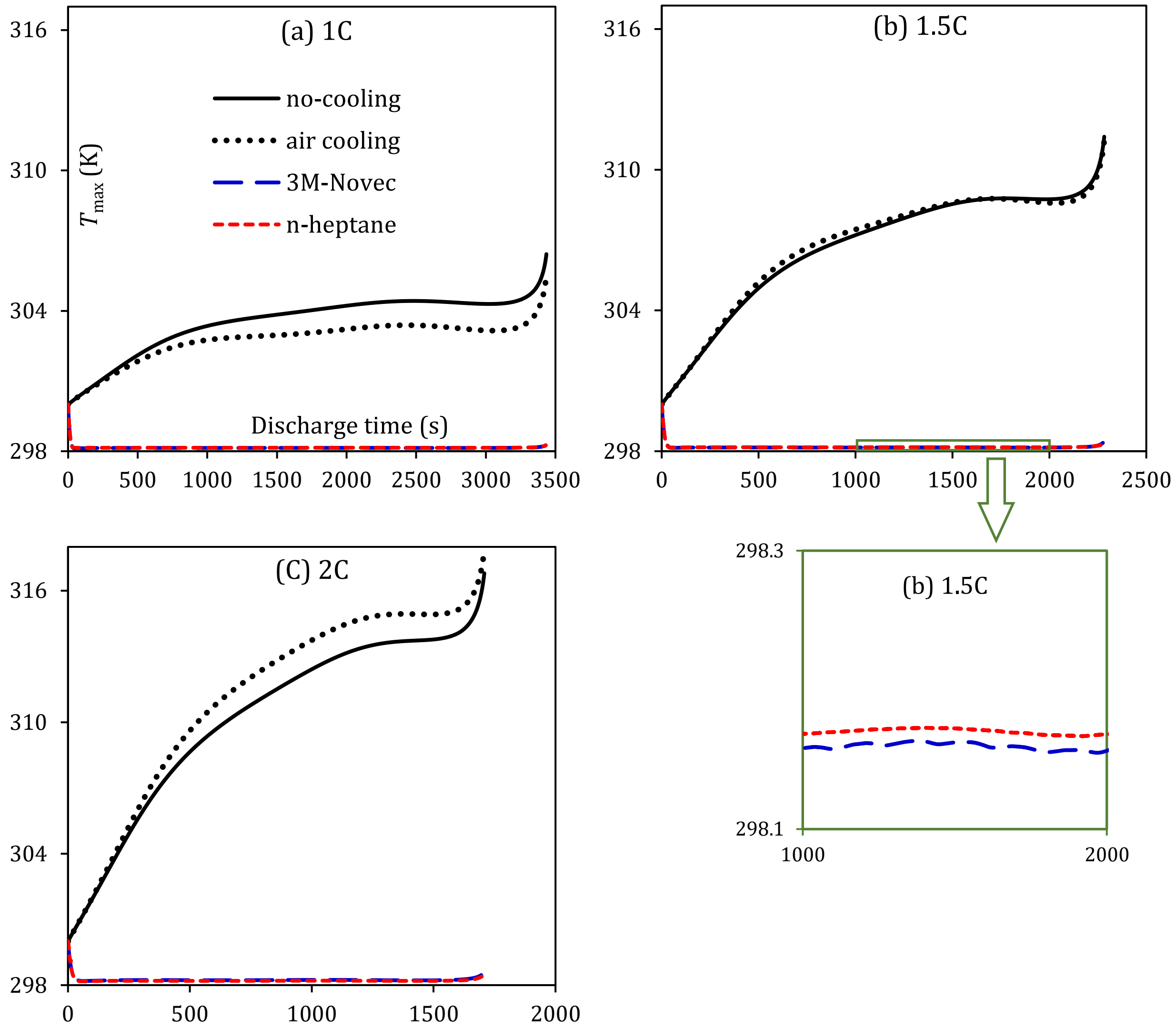

Figure 15. Maximum battery volume temperature versus discharge time at (a) 1C, (b) 1.5C and (c) 2C discharge rates. These were conducted at inlet velocity 0.5 m·s^{-1} for batteries without cooling and cooled using air, 3M Novec, and n-heptane.

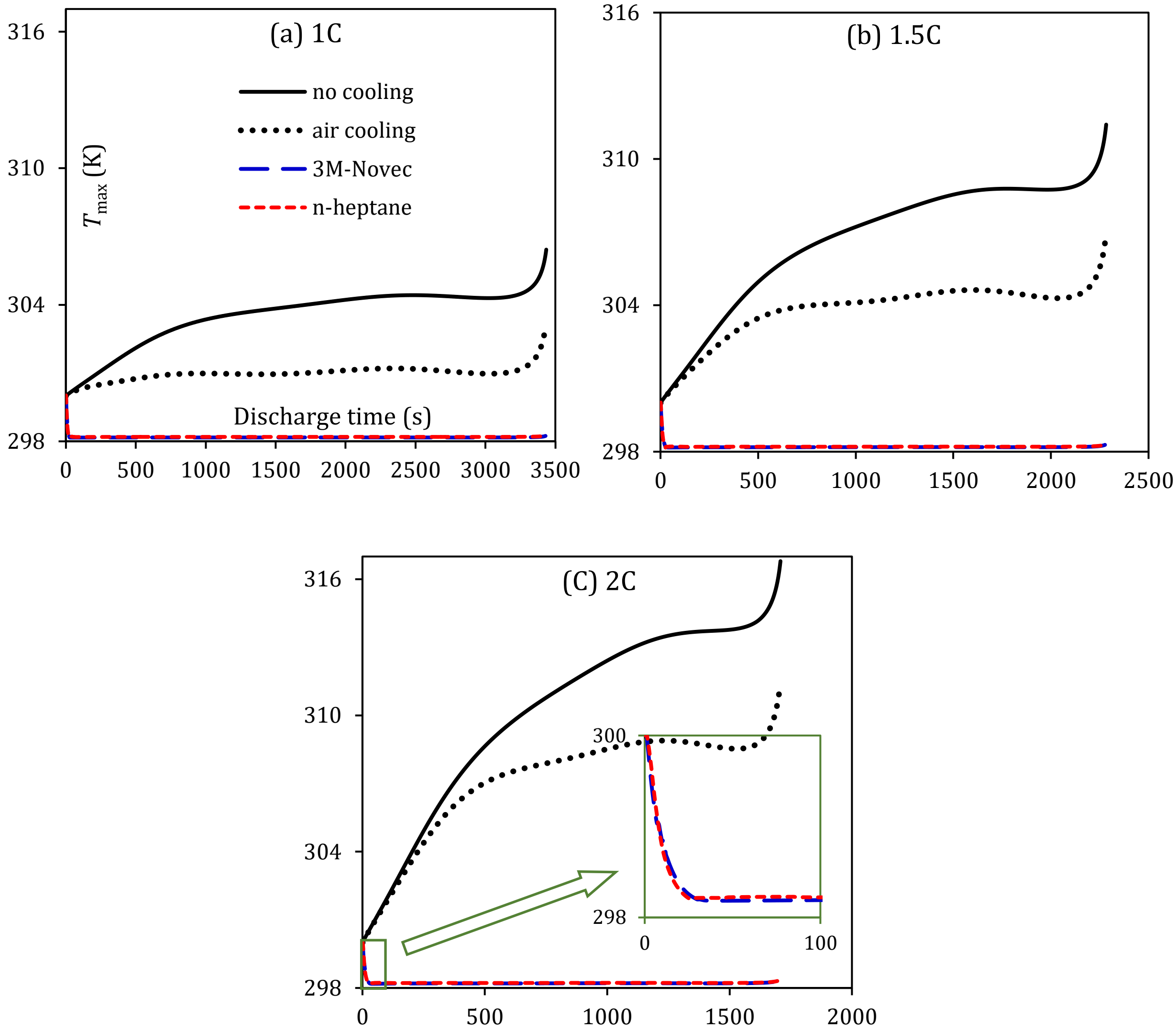

Figure 16. The same as Figure 15, but at 1 m·s^{-1} inlet velocity.